TISSUE TYPE DIFFERENTIATION FOR BRAIN GLIOMA USING NON-NEGATIVE MATRIX FACTORIZATION

Yuqian Li[1,2,3], Diana M. Sima[2,3], Sofie Van Cauter[4,5], Uwe Himmelreich[5], Yiming Pi[1]
and Sabine Van Huffel[2,3]

[1]*School of Electronic Engineering, University of Electronic Science and Technology of China*
Xiyuan Dadao 2006, Chengdu, China
[2]*Department of Electrical Engineering, ESAT-SCD, Katholieke Universiteit Leuven, Leuven, Belgium*
[3]*IBBT-K.U.Leuven Future Health Department, Leuven, Belgium*
[4]*Department of Radiology, University Hospitals of Leuven, Leuven, Belgium*
[5]*Biomedical NMR Unit/Molecular Small Animal Imaging Center, Department of Medical Diagnostic Sciences*
Katholieke Universiteit Leuven, Leuven, Belgium

Abstract: The purpose of this paper is to introduce a hierarchical Non-negative Matrix Factorization (NMF) approach, customized for the problem of blindly separating brain glioma tumor tissue types using short-echo time proton magnetic resonance spectroscopic imaging (^{1}H MRSI) signals. The proposed algorithm consists of two levels of NMF, where two constituent spectra are computed in each level. The first level is able to correctly detect the spectral profile corresponding to the most predominant tissue type, i.e., normal tissue, while the second level is optimized in order to detect two 'abnormal' spectral profiles so that the 3 recovered spectral profiles are least correlated with each other. The two-level decomposition is followed by the reestimation of the overall spatial distribution of each tissue type via standard Non-negative Least Square (NNLS). This method is demonstrated on in vivo short-TE ^{1}H MRSI brain data of a glioblastoma multiforme patient and a grade II-III glioma patient. The results show the possibility of differentiating normal tissue, tumor tissue and necrotic tissue in the form of recovered tissue-specific spectra with accurate spatial distributions.

1 INTRODUCTION

Glioblastoma multiforme (GBM), which is the highest grade of glioma, is the most common and aggressive type of brain tumor in adults. Accurate diagnosis is of utmost importance in guiding therapy and determining prognosis. Magnetic resonance spectroscopic imaging (MRSI) (Brown et al., 1982), which provides both spectral and spatial information, is becoming increasingly popular as an additional non-invasive tool for clinical diagnosis of brain tumors. Since the concentration of metabolites changes under disease conditions, the profile of the measured signal in each MRSI voxel helps to determine the location of abnormal tissue (Howe et al., 2003).

Because of the heterogeneity of GBMs, the tumoral region could consist of several tissue types (Croitor Sava et al., 2011), which represent actively growing tumor, necrosis or normal brain tissue. Lower grade gliomas do not contain necrosis, but are also heterogeneous, e.g., the tumor can present infiltrations into the normal brain tissue. In MRSI, the partial volume effect, i.e., the presence of several tissue types within one voxel, may lead to increased variability in the measured signals. The spectrum corresponding to each voxel can be approximately described as a linear combination of spectra from different constituent tissue types (Su et al., 2008).

Using Non-negative matrix factorization (NMF) to extract main tissue types from the mixed MRSI data was firstly proposed by Sajda and his colleagues (Sajda et al., 2003; Sajda et al., 2004; Du

et al., 2008; Su et al., 2008). They developed a constraint NMF (cNMF) algorithm, which enforces positivity, and incorporate it into a hierarchical decomposition framework to recover physically meaningful spectra using *long* echo time (TE) MRSI signals.

In this paper, we study the applicability of a novel hierarchical NMF method for tissue type differentiation on *short*-TE MRSI data, which is potentially much more challenging than long-TE due to more complex spectral profiles. The proposed algorithm, as described in Section 3, consists of two levels of NMF, where two constituent spectra are computed in each level. Thus, we recover each tissue type step by step using NMF, i.e., first differentiate normal and abnormal tissue, and then, only in the abnormal region, differentiate active tumor and necrosis, or differentiate proliferation level of active tumor if necrosis is not present. Since the choice of the abnormal region has a high influence on the estimated sources, we propose to tune the threshold for selecting the abnormal region by minimizing the correlations between all three estimated tissue spectra, i.e., normal tissue spectral profile from the first-level NMF, and the two abnormal spectral profiles from the second-level NMF. Afterwards, non-negative least squares (NNLS) is applied on the original mixed signals using the obtained spectra in order to reestimate the spatial distribution of each tissue type over the whole grid. In section 4, experimental results on two typical patients show the capability of revealing tissue-specific spectral profiles and their spatial distribution, and are validated against expert labelling.

2 *IN VIVO* 1H MRSI DATA

2.1 Data Acquisition Protocol and Patients

The short-TE MRSI data were acquired at the University Hospital of Leuven (UZ Leuven) on a 3T MR scanner (Achieva, Philips, Best, The Netherlands). Point-resolved spectroscopy (PRESS) (Bottomley, 1987) was used as the volume selection technique, TR/TE: 2000/35 ms, FOV: 16cm*16 cm, volume of interest (VOI): 8cm*8cm, slice thickness: 1cm, acquisition voxel size: 1cm*1cm, reconstruction voxel size: 0.5cm*0.5 cm, receiver bandwidth: 2000Hz, samples: 2048.

Our algorithm was tested on two types of patients:

- *In vivo* MRSI data of GBM patients containing necrotic areas. Anatomic image of a typical patient is shown in Figure. 1(a)
- *In vivo* MRSI data of glioma patients with no apparent necrotic area. Figure 1 (b) shows the anatomic image of a typical patient who has a grade Ⅱ glioma with focal progression to a grade Ⅲ glioma.
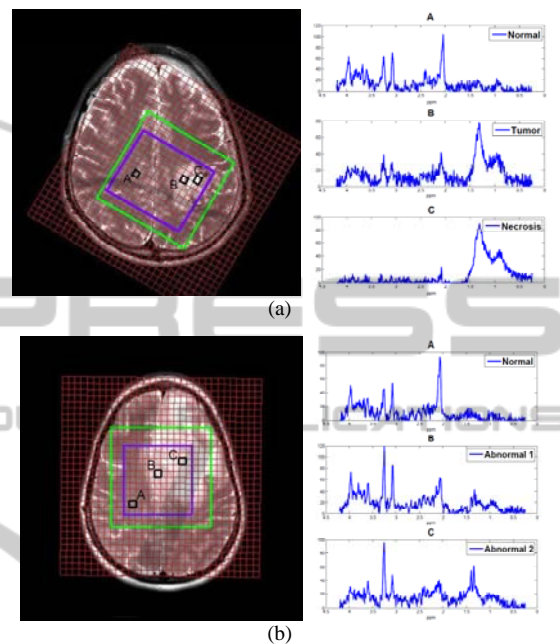

Figure 1: Left: Anatomic image. Right: tissue specific spectra of patients. (a) Patient 1, a GBM patient with necrosis. (b) Patient 2, a glioma patient with no apparent necrosis areas. The outer green box is the PRESS box and the inner blue box contains the selected voxels of interest.

2.2 Data Preprocessing

In-house software SPID (Poullet, 2008), which was developed on the Matlab platform, was used for standard spectroscopic signal preprocessing. The applied steps were as follows:

- In the MRSI grid, signals of insufficient quality (low signal-to-noise ratio (SNR), baseline problems, chemical shift displacement effects, etc.) usually exist, affecting mostly the voxels close to the border of the PRESS box. Therefore, these signals were excluded by selecting an inner smaller box inside the PRESS box of the MRSI grid (see Fig.1).
- Residual water components ware removed using Hankel-Lanczos Singular Value Decomposition with Partial Re-Orthogonalization (HLSVD-PRO) (Laudadio et al., 2002). The model order

was set to 30 and the passband from 0.25 to 4.2 ppm.

- A baseline offset correction was found necessary. But this is not suppressing the baseline due to macromolecules, which may be relevant for tissue differentiation.

- The real parts of the preprocessed spectra were truncated to the region 0.25 – 4.2 ppm before analyzing them using the NMF algorithm.

3   METHODS

3.1   Basics of Non-negative Matrix Factorization (NMF)

NMF (Paatero et al., 1994; Lee et al., 1999), as a blind source separation (BSS) method, has attracted much attention in performing the factorization:

$$X = WH + N \qquad (1)$$

where X is a matrix of observed MRSI spectra represented as column vectors, with one column per voxel. W is a matrix of constituent tissue spectra, with each column representing a typical spectrum for each tissue type. Each row of the matrix H contains the linear combination weights (interpreted here as abundances or concentrations) of all constituent tissue spectra. N stands for additive measurement noise. The mathematical formulation of the basic NMF problem is

$$\min_{W,H} f(W,H) = \frac{1}{2} \| X - WH \|_F^2 \qquad (2)$$
$$subject\ to\ W \geq 0, H \geq 0$$

3.2   Hierarchical NMF-NNLS

In this section, a hierarchical NMF-NNLS algorithm, which recovers the 3 most distinct tissue-specific spectral profiles and their corresponding spatial distributions step by step, is described.

- **Step 1:** First level NMF. Apply NMF to the preprocessed MRSI signals with the number of components chosen to be 2. Two patterns of spectra (*W*-normal and *W*-abnormal, respectively) and their contribution to each location in the brain image (*H*-normal and *H*-abnormal) will be recovered. Then, label the obtained 2 sources as normal and abnormal tissue types according to typical metabolic features of their spectral profiles (i.e., the NAA

peak at 2.01 ppm is higher in the source corresponding to normal tissue).

- **Step 2:** Automatically find the optimal threshold for the abnormal region. Perform intermediate NMF decompositions with 2 sources on gradually increasing sets of voxels, where these sets are selected according to a variable threshold on the magnitude of the *H*-abnormal map. A reasonable trade-off for mutually least correlation between recovered spectral profiles is found by minimizing the sum: *Corr(W-normal,W*-abnormal1) + *Corr(W*-normal,*W*-abnormal2) + *Corr(W*- abnormal1+*W*-abnormal2).

- **Step 3:** Second level NMF. Apply NMF only to the voxels of the abnormal region selected using the optimal threshold in order to further separate the abnormal tissue into two abnormal tumor profiles, which reflect the aggressiveness level, with their corresponding spatial distributions. If one of the profiles contains predominantly lipids (according to the peaks at 0.9 and 1.3 ppm) and almost no other metabolites, then label that profile as necrosis.

- **Step 4:** NNLS reestimation. Since the second level NMF was restricted to the selected abnormal region, some border voxels containing abnormal tissue may have been excluded due to the thresholding. Applying non-negative least squares approach (Lawson et al., 1974) to the whole grid with the 3 recovered tissue spectra (i.e., solving problem [2] for *W* fixed to a three-column matrix [*W*-normal, *W*-abnormal1, *W*-abnormal2]) will give a complete estimation of the spatial information of these 3 tissue types over the whole initially considered grid.

4   EXPERIMENTAL RESULTS

We studied the applicability of brain tumor tissue type differentiation using the proposed hierarchical NMF-NNLS algorithm. The results of two different cases are shown in Figure 2 and Figure 3.

4.1   Results for Patient 1: GBM Patient with Necrosis

Results of 2-level hierarchical NMF-NNLS to the preprocessed brain signals of patient 1 are shown in Figure 2. The corresponding anatomic picture of the patient 1 (male, GBM) is shown in Figure 1 (a) with the green box and the blue box representing the

PRESS box and the selected voxels of reasonable quality, respectively. Figure 2 (a) presents the recovered normal and abnormal spectra of the first level NMF. The spectrum that shows a decreased NAA/Cho ratio, a decreased Cre and significant levels of Lac-Lip, represents the tumor tissue. The one with almost no metabolites other than lipids (and potentially lactate), is the typical spectral pattern of necrotic tissue. The *H*-maps in (b) give their spatial distribution. (c) illustrates the selected abnormal region. (d) and (e) are the results of the second level NMF. (f) shows the reestimated spatial information using NNLS. We can see tumor and necrosis in (c) covering bigger regions than in (b) and therefore being able to show more complete information at the border region which contains mixed tissues.

4.2 Results on Glioma Patients with no Apparent Necrosis Area

To explore the applicability of the proposed method (see Section 2.4), it was tested on another case, which is a patient who has been diagnosed with grade II-III glioma and, according to the expert labeling, does not present macroscopic necrosis; Anatomic picture is given in Figure 1 (b). Results are shown in Figure 3. It is controversial if we still try to search for 3 components with our method when there is no necrosis. Still, this situation is realistic, because in most cases we are not sure beforehand if there is necrosis within the lesion.

Figure 3 (a) and (b) give the results of the first level decomposition and thresholding. Panel (a) illustrates the recovered spectra of normal tissue and abnormal tissue; the *H*-maps in (b) show the spatial distribution of the corresponding spectra after
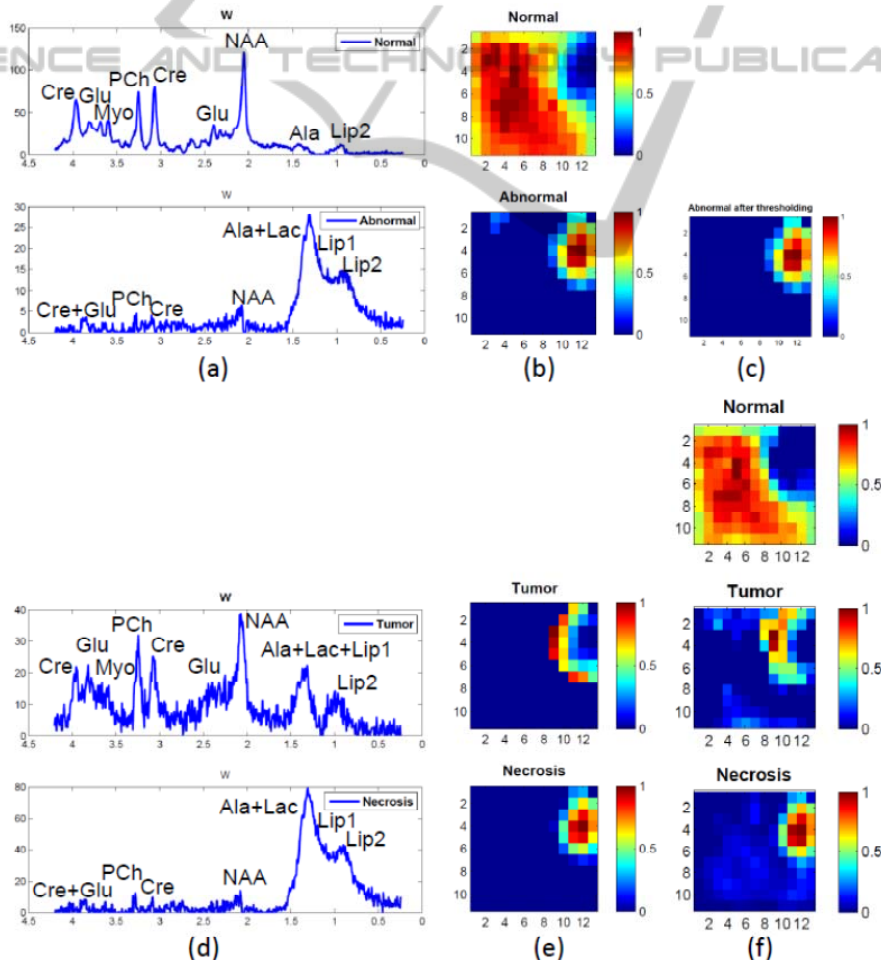

Figure 2: Result of hierarchical NMF-NNLS on patient 1, a GBM patient with necrosis. (a) – (b): Step 1, first level NMF. (c): Abnormal region after optimal thresholding. (d) – (e): Step 3, second level NMF. (f): Step 4, NNLS.

thresholding. We can see that the factorization is effective in finding normal and abnormal tissue.

Then, in Step 3, the abnormal tissue was separated into two parts that apparently do not contain necrotic tissue (also confirmed by the absence of lipids). The one near the normal region is the border of the tumor, with its spectral pattern (Abnormal 1 in Figure 3 (c)) still indicating abnormality (low NAA/Cho). The recovered spectrum from the other part of abnormal region (Abnormal 2 in Figure 3 (c)) has a significant increase of Cho and Lips, obvious peaks of Ala and Lac, and a decrease of other metabolites. For this case without necrosis, instead of separating tumor and necrosis, our proposed method reveals the regions in the tumor that correspond to different levels of proliferating tumor cells. In the end, NNLS estimation gives more complete spatial information of each tissue type.

4.3 Results Validation

The distribution maps of the 3 tissue types were overlapped onto the anatomical images; see Fig. 4. The recovered location of our results corresponds well to the one shown on the anatomic image.

As an additional validation for patient 1, we also computed correlation coefficients between the recovered spectra and the average of pure tissue-specific spectra according to the labeling of an expert (SVC). The result for normal tissue is 0.9933, for tumor is 0.9618 and for necrosis is 0.9950, which shows that all spectral sources are relatively highly correlated with the validated spectra.

For patient 2, who has grade II-III glioma but without macroscopic necrosis, the result of our proposed method reflected the level of tumour proliferation, which was validated by histopathology.
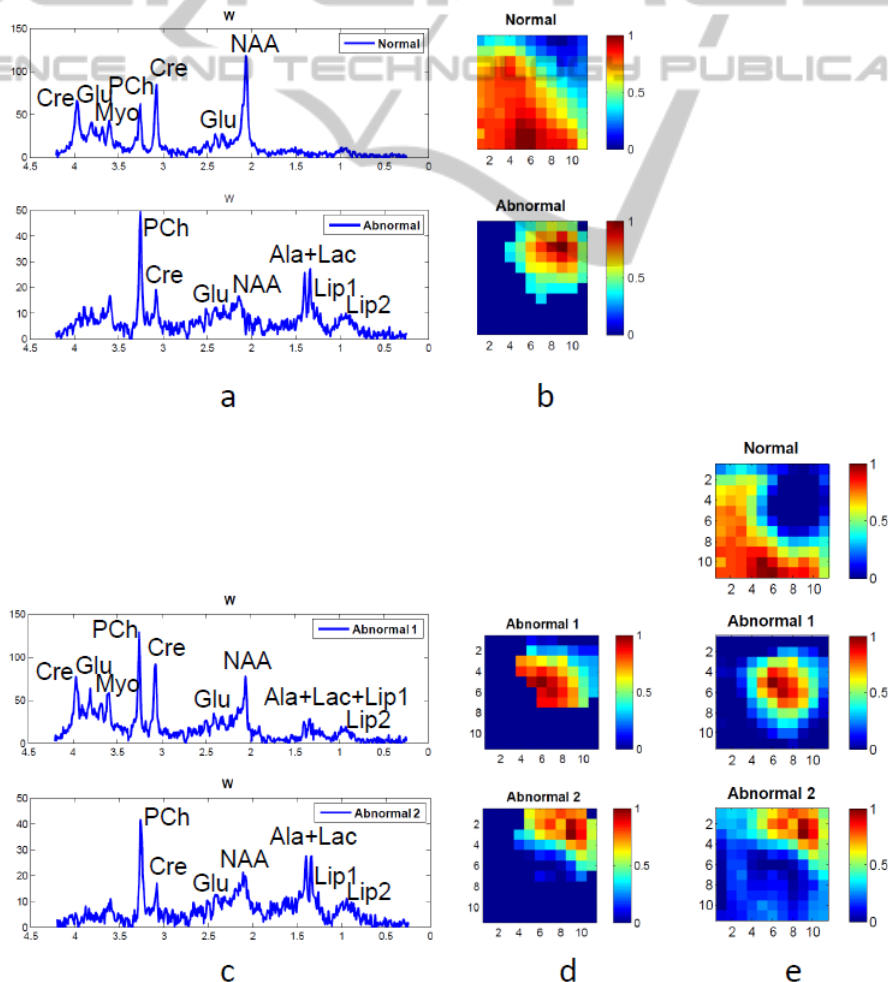

Figure 3: Result of hierarchical NMF-NNLS on patient 2, a glioma patient with no apparent necrosis area. (a) – (b): Step 1-2, first level NMF and optimally selected abnormal region (c) – (d): Step 3, second level NMF. (e): Step 4, NNLS.
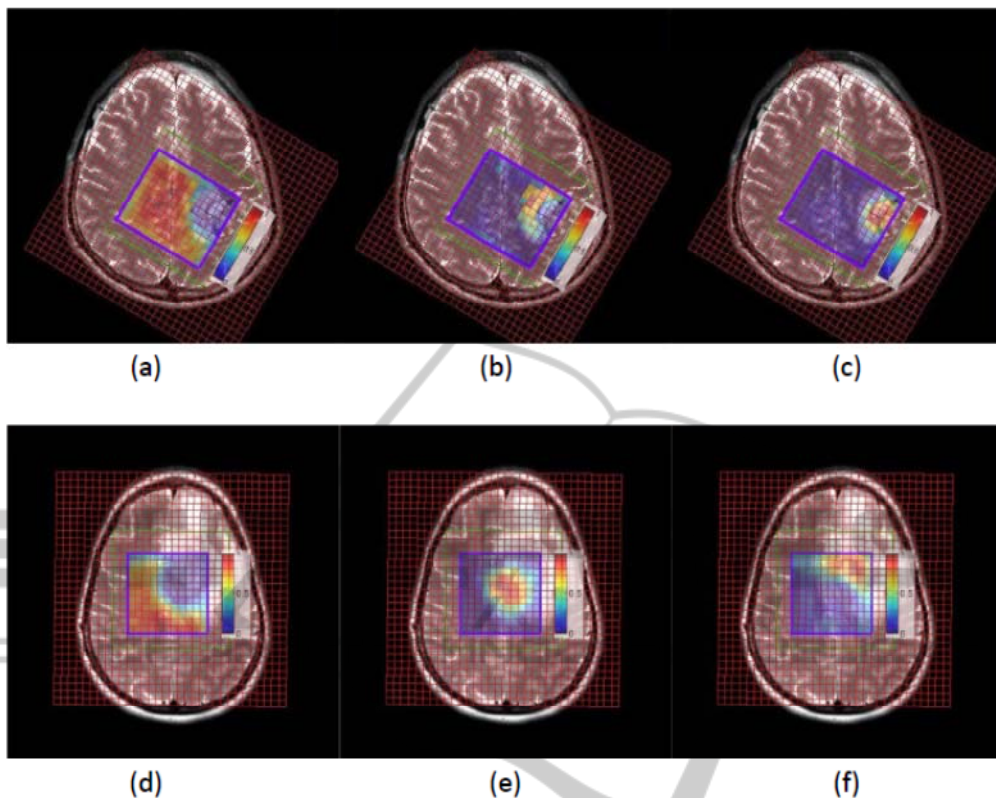
Figure 4: Overlap of the distribution results onto the anatomic images. The first row is the result of the GBM patient with necrosis. (a): normal tissue distribution; (b): tumor tissue distribution; (c): necrosis tissue distribution. The second row is the result of the glioma patient without necrosis. (a): normal tissue distribution; (b): abnormal 1 tissue distribution; (c): abnormal 2 tissue distribution.

5 DISCUSSION & CONCLUSIONS

A novel tissue type differentiation approach, hierarchical NMF-NNLS, and its clinical application were explored in this study for GBM patients.

The data we used in this study is *short*-TE MRSI signals because spectra of short-TE represent more metabolites than long-TE spectra. But there is more significant peak overlap and, usually, a higher noise level. Therefore, using short-TE signals in solving tissue type differentiation is more challenging but of more significance.

The reason we need the hierarchical procedure is based on the assumption in the considered data sets that the MRSI grid encompasses mostly normal tissue and a glioma tumor with heterogeneous tissue content. Due to the unbalanced proportion of the tumor tissue voxels inside the grid, the sources corresponding to under-represented tissue types would be difficult to be identified by simply using NMF with more than 2 sources. Therefore, the robustness of NMF for extracting meaningful spectral patterns can be increased through a hierarchical NMF approach.

The possibility of differentiating brain tumor tissue types was demonstrated in two distinct cases. Representative results from a GBM patient showed the capability of the proposed algorithm to separate short-TE MRSI data into normal tissue, tumor and necrosis with accurate spatial information. For the case of a glioma patient without necrosis, our method is able to indicate the proliferation level of the tumor. This result is useful because assessing tumor proliferation level is important in brain tumor diagnosis, as it gives information that is potentially helpful in directing the patient's clinical management. Both cases show that the proposed method is able to find meaningful sources and their corresponding spatial distributions using short-TE MRSI signals.

However, the data presented in this paper is preliminary and a more appropriate data pool will be

used in future work in order to actually fully assess the performance of the proposed technique.

Another paper appearing in these proceedings focuses on a "simulation study of tissue type differentiation using non-negative matrix factorization". In that preliminary research, we studied the performance of several NMF implementations on simulated MRSI signals. The '(a)hals' algorithm (Cichocki et al., 2007; Cichocki et al., 2009; Gillis, 2011) had the best performance in those simulations and has therefore been used for all the NMF computations in this paper.

ACKNOWLEDGEMENTS

REFERENCES

Bottomley PA, 1987. Spatial localization in NMR-spectroscopy in vivo. *Ann N Y Acad Sci*, 508:333–348.

Brown T, Kincaid B, Ugurbil K, 1982. NMR chemical shift imaging in three dimensions. *PNAS*, 79(11): 3523-3526.

Croitor Sava A, Martinez-Bisbal MC, Van Huffel S, Cerda JM, Sima DM, Celda B, 2011. Ex vivo high resolution magic angle spinning metabolic profiles describe intratumoral histopathological tissue properties in adult human gliomas. *Magn Reson Med,* 65:320-328.

Cichocki A, Zdunek R, Amari S, 2007. Hierarchical ALS algorithms for nonnegative matrix and 3D tensor factorization. *Lect Notes Comput Sci*, 4666:169-176.

Cichocki A, Phan AH, 2009. Fast local algorithms for large scale Nonegative Matrix and Tensor Factorizations. IEICE Trans Fund Electron *Comm Comput Sci*, 3:708-721.

Du S, Mao X, Sajda P and Shungu DC, 2008. Automated tissue segmentation and blind recovery of 1H MRS imaging spectral patterns of normal and diseased human brain. *NMR in Biomedicine,* 21:33-41.

Gillis N, 2011. *Nonnegative matrix factorization complexity, algorithms and applications*. PhD Thesis, Louvan-La-Neuve, Belgium.

Howe FA, Barton SJ, Cudlip SA, Stubbs M, Saunders DE, Murphy JR, Opstad KS, Doyle VL, McLean MA, Bell BA, Griffiths JR, 2003. Metabolic profiles of human brain tumours using quantitative in vivo 1H magnetic resonance spectroscopy. *Magn Res Med,* 49:223-232.

Laudadio T, Mastronardi N, Vanhamme L, Van Hecke P, Van Huffel S, 2002. Improved Lanczos algorithms for blackbox MRS data quantitation. *J Magn Reson,* 157: 292-297.

Lawson C.L. and R.J. Hanson, 1974, Solving Least-Squares Problems, Prentice-Hall, Chapter 23, p. 161,.

Lee DD, Seung HS, 1999. Learning the parts of objects by non-negative matrix factorization. *Nature,* 401:788-791.

Paatero P, Tapper U, 1994. Positive matrix factorization: A non-negative factor model with optimal utilization of error. *Environmetrics,* 5:111-126.

Poullet JB, 2008. *Quantification and classification of magnetic resonance spectroscopic data for brain tumor diagnosis.* PhD Thesis, Leuven, Belgium.

Sajda P, Du S, Brown TR, Parra LC, Stoyanova R, 2003. Recovery of constituent spectra in 3D chemical shift imagin using non-negative matrix factorization. *In Proc. 4th Int. Symp. ICA and BSS,* 71-76.

Sajda P, Du S, Brown TR, Stoyanova R, Shungu DC, Mao X, Parra LC, 2004. Nonnegative Matrix Factorization for Rapid Recovery of Constituent Spectra in Magnetic Resonance Chemical Shift Imaging of the Brain. *IEEE Trans Med Imaging*, 23:1453-1465.

Su Y, Thakur SB., Karimi S, Du S, Sajda P, Huang W, Parra LC, 2008. Spectrum separation resolves partial-volume effect of MRSI as demonstrated on brain tumor scans. *NMR Biomed,* 21:1030-1042.